Research Article

Conjoint Influence of Heat Treatment, Hot Deformation and Cold Working on the Microstructure and Mechanical Response of a Co-Based Superalloy

S.M. Arab[1*], A. Haghighi[2], M. Khajepour[3], Y. Jalalizadeh[4] and M.M. Tavallayi[5]

[1] Department of Mechanical Engineering, University of Mohaghegh Ardabili, P.O. Box 179, Ardabil, Iran
[2] School of Metallurgy and Materials Engineering, University of Tehran, Tehran, Iran
[3] Department of Materials Engineering, Shahid Bahonar University of Kerman, Kerman, Iran
[4] School of Metallurgy and Materials Engineering, Sahand University of Technology, Tabriz, Iran
[5] Department of Electroceramics, Faculty of Materials Engineering, Shiraz University of Technology, Shiraz, Iran

ARTICLE INFO

ABSTRACT

An as-cast HAYNES 25 Co-based superalloy is subjected to a process, including four stages of heat treatment, hot deformation, cold working, and aging. Mechanical properties have been improved after processing; the hardness, tensile and yield strengths are enhanced while the reduction of ductility is reasonable. The process has led to break down the segregated as-cast microstructure and has given a well distributed inter-metallic reinforced microstructure with no segregation. The grain structure also includes the approximately equiaxed grains with a large density of $\Sigma3$ twins. The results showed that as the hot deformation plays an important role in the grain refinement and microstructure homogenization, it should be considered as an important phase of the manufacturing process.

1. Introduction

Among the various types of heat resistant alloys, wrought Co-based superalloys have been widely used in high temperature applications, which need to keep up the strength, resistance to fatigue, creep, and especially resistance to wear and hot corrosion attacks [1]. The HAYNES 25 alloy (cobalt-nickel-chromium-tungsten alloy which is also known as L-605) development has a seventy-year history. The ordered criterion was high rupture lives at high temperatures for military applications. Until the recent advances, HAYNES 25 has the highest creep strength among the fabricated superalloys. It has good resistance to oxidizing environments up to 1000ºC for prolonged exposures. It also has excellent resistance to degradation induced by sulfur [2]. Additionally, it is well-known for its high resistance to wear and galling. The HAYNES 25 alloy has been used in many applications such as gas turbine components, including combustors, rings, seals, and blades. It has also found applications in heart valves [3], balls and bearings, forging dies, and a variety of industrial heating applications [4]. Based on the history of the material (cold work percentage, initial grain size, etc.), the solution treatment temperature for HAYNES 25 varies

---

from 1175-1230°C. It should be noted that higher temperatures lead to larger grain size after solution heat treatment [5]. There are a few studies on the hot working and cold deformation and heat treatment of HAYNES 25 superalloy. M. Kenzevic et al. [6] investigated the deformation behavior of Co-based superalloy, HAYNES 25. They observed no evidence of deformation twinning but found the stacking faults which occur within the grains as the main defect strengthening mechanism. During the cold deformation of the Co-based superalloys, failure occurs because of adiabatic shearing along the planes with higher resolved shear stress, such as the planes which are oriented at angles of 40°-50°. The dislocation density and the flow stress are strongly dependent on the forming temperature and strain rate. As the strain rate and strain increase and the temperature decreases, the interaction between the dislocation themselves and dislocations and the band-like structure in the grains increases, which results in higher hardness and tensile strength [7]. An increase in the cold work percentage reduces the elongation and enhances the hardness and yield stress [8]. A high density of stacking faults within the grains is reported as the responsible mechanism controlling the mechanical behavior of the alloy [6].

A kind of FCC to HCP transformation can take place during the plastic deformation of Co-based superalloys [9]. It is owing to the glide of Shockley partials on the {111} planes, which also contributes to the plastic deformation [10] or accumulation and coalescence of stacking faults [11].

The aging and solution treatment times are also effective parameters that influence the precipitation hardening efficiency and final mechanical properties. J. Favre, et al. [12] have suggested a very short time annealing procedure to prevent the grains from coarsening. They reached metastable statically recrystallized fine grains, which transform to coarser fully recrystallized grains in a couple of seconds. In this study, it has been tried to use different combinations of solution treatment, hot deformation, cold working, and age hardening to investigate the effect of processing parameters on the microstructure and mechanical properties of the HAYNES 25 alloy. The main goal is to prevent the alloy from macro and micro-segregation, to obtain finer grains through dynamic recrystallization, and to reach the higher hardness and strengths by cold working and age hardening.

2. Materials and Methods

An as-cast HAYNES 25 alloy disk with 80 mm in diameter has been used to extract the samples for solution treatment, hot working, cold working, and precipitation hardening. The chemical composition of the as-received alloy is given in Table 1. First, disks with 60 mm of diameter and 14 mm of thickness have been wire-cut. Solution treatment has been carried out under the circumstances given in Table 2 based on the literature [13].

Table 1. Chemical composition of the as-received HAYNES 25 alloy

Element	Co	Cr	W	Ni	Fe	Mn	Mo	Si	C	S	P
wt.%	bal	20.00	13.4	12.1	3.54	1.48	0.12	0.15	0.08	0.015	0.015

Table 2. The different conditions for solution treatment of as-received samples

Treatment code	Temperature (ºC)	Holding time (min)	Cooling media
H1	1230	15	25ºC water
H2	1230	30	25ºC water
H3	1280	15	25ºC water
H4	1230	60	25ºC water

Table 3. The hot deformation condition for HAYNES 25 samples

Hot forging code	Forging temperature (ºC)	Eng. strain (%)	Preheat time (min)	Preheat temperature (ºC)	Cooling media
HF1	1075	15	20	1100	Air
HF2	1075	30	20	1100	Air
HF3	1075	60	20	1100	Air
HF4	1175	15	20	1200	Air
HF5	1175	30	20	1200	Air
HF6	1175	60	20	1200	Air
HF7	1275	15	20	1300	Air
HF8	1275	30	20	1300	Air
HF9	1275	60	20	1300	Air

Table 4. Post-deformation aging condition for HAYNES 25 samples

| Treatment code	Temperature (ºC)	Holding time (h)	Cooling media
Age1	430	3.5	Air
Age2	430	10	Air
Age3	430	24	Air
Age4	480	24	Air

After solution treatment, the mechanical properties and microstructure of samples were studied. Based on the specified requirements, the optimum condition of solution treatment is selected. Then, hot and cold working, and post-aging heat treatment have been applied on the as-received and solution treated samples. The condition for hot forging, cold forging, and artificial aging are indicated in Tables 3 and Table 4. The amount of cold work is 20% by cold upsetting based on the required specifications and literature [14]. After deformation, before and after aging, the microstructure of the samples has been studied through optical and scanning electron microscopy (SEM and FESEM-MIRA3 TESCAN at RMRC). The grain size is measured based on ASTM E12 through the planimetric method. Mechanical properties are achieved by tensile, impact, and hardness testing. The stress-strain data, impact toughness, and microhardness examinations have been obtained based on the ASTM E8, ASTM E23, ASTM E18, and ASTM E384, respectively.

3. Results and Discussion

3.1. Microstructural studies

Fig. 1 shows the microstructure of as-cast material. Intensive micro and macro-segregation are quite clear in the microstructure. The alloying elements have been
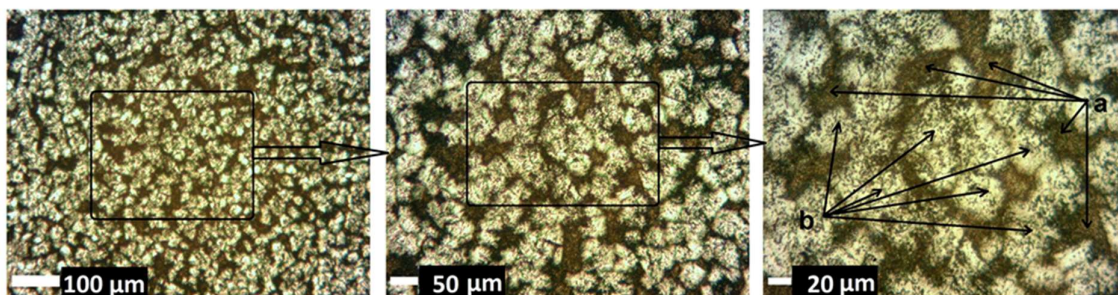
Fig. 1. The microstructure of as-cast HAYNES 25 alloy.

segregated in the grain boundaries (Fig. 1- a (darker) regions) and into the wide areas of the grains (Fig. 1- b (brighter) regions).

The EDS analysis of FESEM images indicates that the WC (blocky carbides) and W_6C carbides have been segregated into the grains and $Cr_{23}C_6$ carbides are segregated into the grain boundaries (Fig. 2).

If the blocky carbides are large and service or heat treatment temperature is high enough, the blocky WC carbides combine into their surrounding base metal and decompose to the W_6C ones. Considering the carbon, tungsten and cobalt peaks and their ratio in Fig. 2(b) and the W-C-Co ternary phase diagram (Fig. 3). If this is achieved, it can be concluded that there might be another intermetallic precipitation such as $Co_6W_6C_y$ and $Co_3W_3C_y$ which are similar to the $M_{12}C$ and M_6C [15]. Chromium improves resistance to the oxidation in addition to producing the strengthening precipitations. Molybdenum and tungsten strengthen the matrix through the solid solution and second phase

precipitation. Therefore, if they segregate, they cannot play the roles which they are responsible for in the microstructure and mechanical properties [1]. The $M_{12}C$ carbides are more coherent with the matrix in comparison with the MC and M_6C carbides [16].

This inhomogeneous microstructure leads to non-uniform mechanical, wear and corrosion properties which influence the material performance [14]. In order to eliminate the harmful segregation, solution treatment was done on the as-received samples. The microstructures of the solution treated samples are shown in Fig. 4. If the solution heat treatment is done well, there would be no laves and sigma phases, namely, the harmful precipitations which lower the ductility and the toughness. In such conditions, the mentioned phases cannot be formed even at the long aging phase [17]. The casting segregation can be eliminated, but, at the same time, the grain growth would take place. The mean grain size has been increased from 70 μm for the as-cast sample to 72 μm for H1, 78 μm for H2, 96 μm for H3,
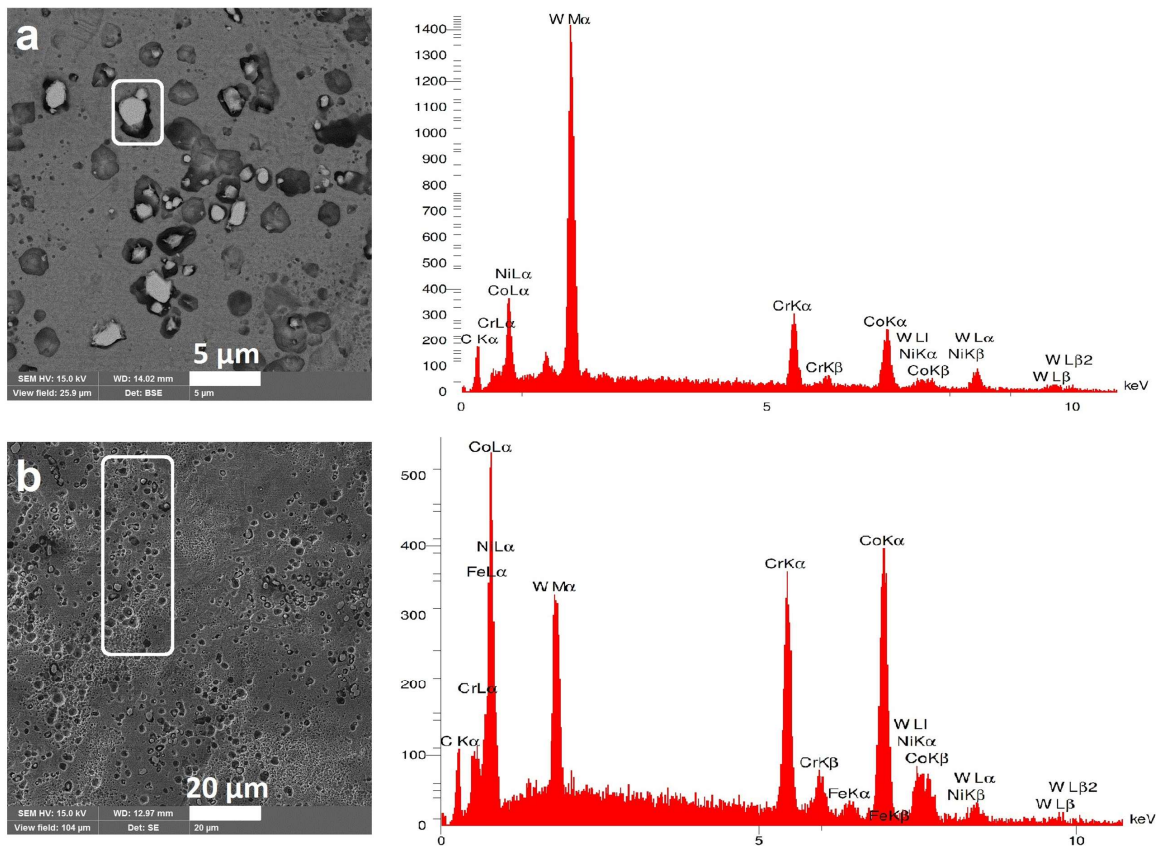

Fig. 2. The FESEM images of (a) granular and (b) intergranular segregation of as-cast HAYNES 25 alloy.
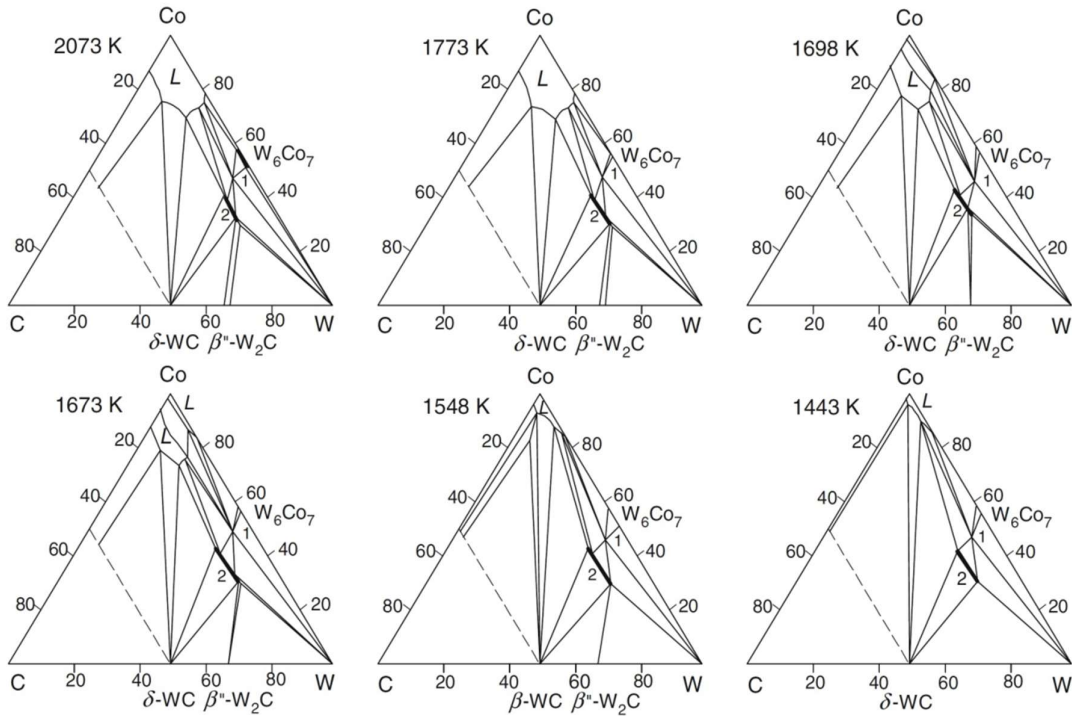
Fig. 3. The isothermal phase equilibria in the W–Co–C System at different temperatures. Line 1 shows $W_6Co_6C_y$ carbide and line 2 shows $W_3Co_3C_y$ solid solution [15].

and 80 μm for H4 condition.

Therefore, it can be concluded that the higher solution treatment temperature enhances the grain size more than the longer holding time. There is not a significant amount of remaining precipitation in the H1 leads to dissolving some of the particles on one hand, and growing some other particles, especially in the grain and twin boundaries (see the circles and arrows in Fig. 4)
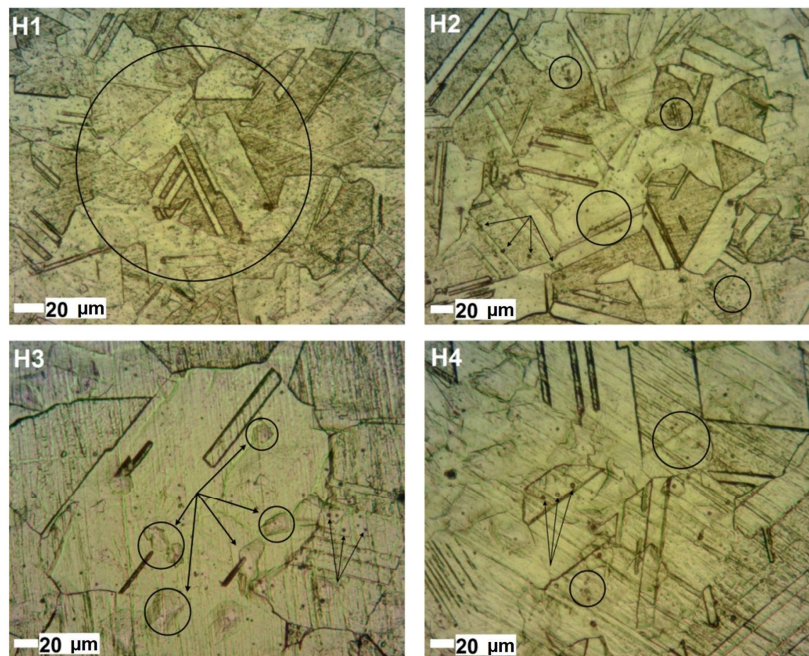

Fig. 4. The microstructure of HAYNES 25 alloy under different solution treatment conditions. H1 to H4 conditions are referred to Table 2.

on the other hand. Higher temperatures (H3) and longer exposure times (H4) increase the remaining particle size as well as the grain size. The coarse precipitations along with coarse grains cannot pin the dislocations and grain boundaries to keep the strength under high temperature working conditions to satisfy the strengthening requirement. Therefore, it is better to choose the lower temperatures in addition to shorter heat treatment times, which can dissolve the majority of the precipitations without remarkable particles and grain growth.

Another characteristic of the alloy after solution heat treatment is the occurrence of numerous twinning. These twins are introduced as the $\Sigma 3$ annealing twins that have a boundary angle of 60°. These twins are especially formed in the coarse grain structure [18] and might be created from geometrical interactions between the pre-existing $\Sigma 3$ boundaries. They also can be a source for the next generation of $\Sigma 9$, $\Sigma 27$ and $\Sigma 3$ twins during the further deformation and recrystallization process [19].

Fig. 5 indicates the microstructure of hot forged samples mentioned in Table 3. An increase in the strain leads to grain size reduction due to dynamic recrystallization (DRX) [20]. Dynamic recrystallization is reported as the predominant grain refinement mechanism during hot deformation. In addition to the conventional dynamic recrystallization mechanisms, the particle stimulated nucleation (PSN) mechanism increases the nucleation rates and produces finer grains. The nucleation sites can be the M_6C and $M_{23}C_6$ particles which have remained after solution treatment or precipitated during the heat-up before hot deformation [12]. Nonetheless, because of the power law between σ-Z (stress and Zener-Hollomon parameter) with high value of the stress exponent (n) and activation energy (Q), grain refinement could be carried out at higher Z values (lower temperatures and higher strain rates) and grain coarsening would take place at lower Z values. Dynamic recrystallization also enhances the ductility
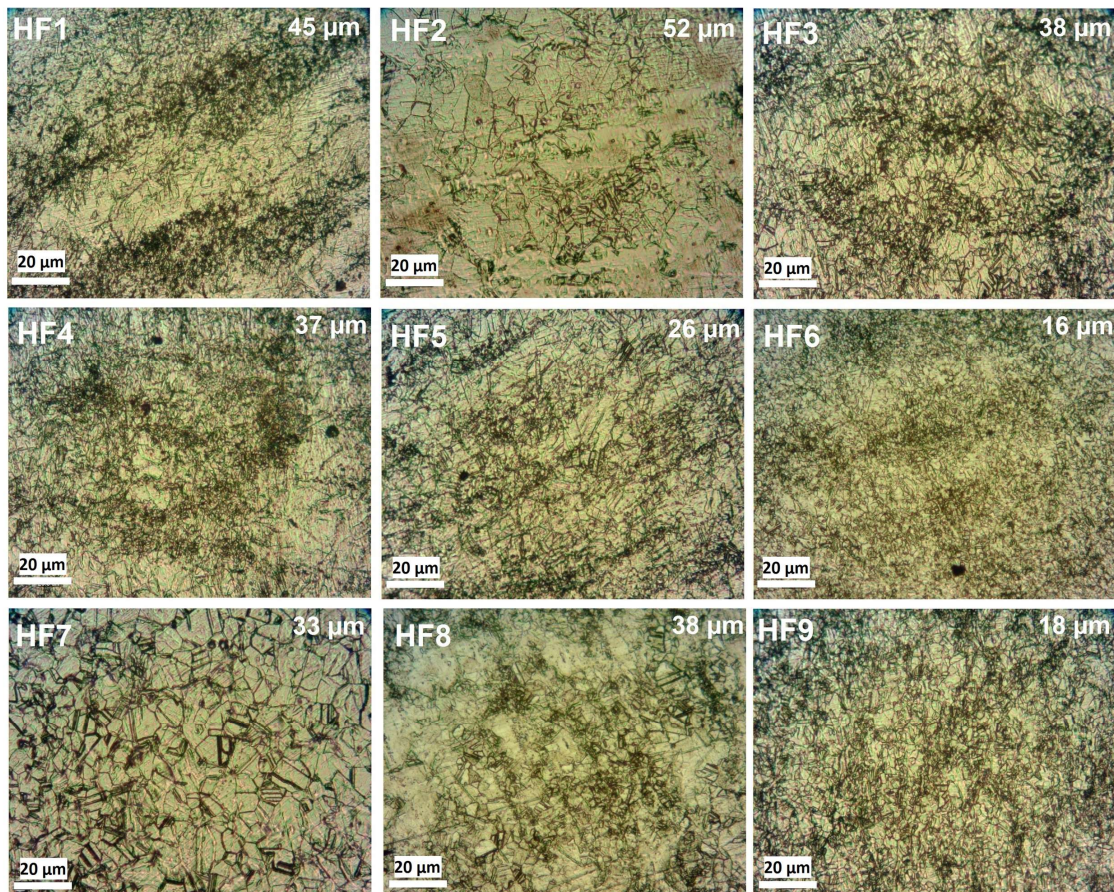

Fig. 5. The microstructure of hot forged HAYNES 25 samples under different conditions. HF1 to HF9 conditions refer to Table 3.

and, therefore, workability at high temperatures [21]. The finer grains show lower propensity for twinning. It is attributed to a change in the deformation mechanism from twinning to the slip with grain size reduction. This can be explained using the Hall-Petch relationship. Both twinning and slip get harder with grain refinement, but because the relationship slope for twinning is higher than that of the dislocation slip, the twinning becomes more and more difficult than slip [22, 23]. Grain size resulting from hot deformation has an important effect on the mechanical properties of HAYNES 25. Grain refinement leads to enhancement of yield stress, tensile strength and Rockwell hardness. Based on the specified requirement, grain size should be about 35 μm to fulfill the desirable properties for designing applications [24]. As an explanation for Fig. 5, increasing the hot forging temperature to some extent might decrease the grain size. It is related to the activation of dynamic recrystallization. This phenomenon takes place between HF4-HF1, HF5-HF2 and, HF6-HF3, similarly. This could be explained by considering some parameters simultaneously. The recrystallization has an optimal condition to take place in the maximum possible amount. At high strain rates, higher temperatures could result in higher amounts of recrystallization and consequently finer grain structures. At temperatures higher than the optimum temperature, grain growth will take over the refining process [18].

Increasing the temperature, decreases the material's flow stress and allows its deformation and recrystallizes it more easily. Very high temperatures activate the dynamic grain growth, which leads to a more equiaxed grain structure with larger grain sizes than that of the middle hot working temperatures [20]. As there was an industrial target to obtain the uniform grain size of 30-34 μm without remarkable amounts of dynamically precipitated particles, the HF7 is selected as the desired hot deformation condition. Fig. 6(a) indicates the FESEM image of 20% cold worked sample after H1 solution treatment, Fig. 6(b) represents the microstructure of 20% cold worked sample after HF7 hot forging without initial H1 solution treatment and Fig. 6(c)
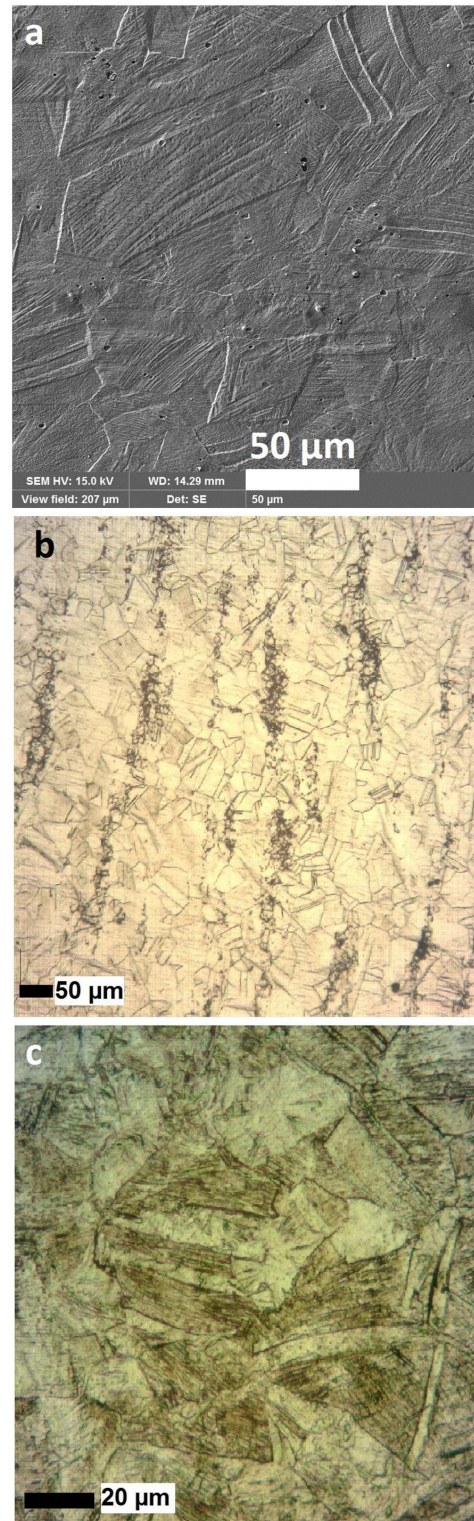

Fig. 6. The microstructure of (a) 20% cold worked sample after H1 solution treatment, (b) 20% cold worked sample after HF7 hot forging without initial H1 solution treatment and (c) 20% cold worked sample after H1 solution treatment and HF7 hot forging.

shows the microstructure of 20% cold worked sample after H1 solution treatment and HF7 hot forging, respectively. The HF7 condition has been chosen because it has satisfied the grain size requirement for a special industrial application and shown no micro and macro-segregation.

As seen, solution treatment and further cold working (Fig. 6(a)) give a uniform microstructure which shows approximately equiaxed grains in addition to the twins with curved boundaries. The grain size does not meet the required grain size (from an industrial application specification) because there was no hot deformation and, therefore, no dynamic recrystallization. Although the hot forged samples without solution treatment (Fig. 6(b)) shows a uniform grain size distribution, there are some parallel zones which shows macro and micro-segregation. These can be attributed to the very short time of the hot deformation processing, which does not allow the alloying atoms to diffuse in the matrix to annihilate the segregation. The formation of thin films of continuous chromium carbide in the grain boundaries during hot deformation and heat treatment should be avoided, because it reduces the ductility and facilitates crack initiation and propagation along the carbide thin film during further service operation or cold working [25]. Therefore, it seems to be necessary to carry out the solution treatment before hot deformation. The H1-HF7-20% cold worked sample satisfied the requirements (Fig. 6(c)). It has a finer equiaxed grain structure without any evident macro or micro-segregation which seems to be able to give the expected mechanical properties. Cold working increases the dislocation density, creates the primary twins and results in twins intersection, which leads to strength enhancement and reduction of elongation [26]. Many of the newly formed twins are formed by geometrical interactions between pre-existing twins, in contrast to the hot deformation.

Fig. 7 shows the microstructure of the samples mentioned in Table 4 after H1+20% cold work+Age1 (Fig. 7(a)) and after H1+HF7+20% cold work+Age1 treatment (Fig. 7(b)). It is clear that the process following H1 and HF7 treatment can give a uniform
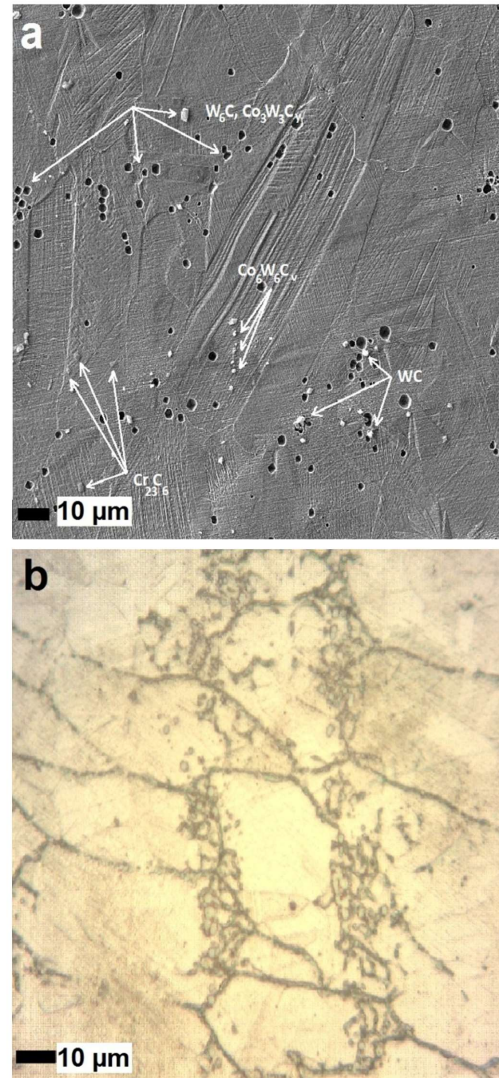

Fig. 7. The microstructure of (a) 20 H1+HF7+20% cold work+ age 1, and (b) H1+20% cold work+age 1.

microstructure with finer grain size than the samples which have not experienced hot forging. It could be concluded that the blocky black holes belong to the particles which commonly have blocky shapes such as W_6C and $Co_3W_3C_y$ components.

Very long aging times or higher aging temperatures lead to the elimination of the strengthening effect of cold work as well as precipitation growth. It also increases the hardness of samples by getting to the aging diagram's peak. The grain growth also takes place at higher exposure times and temperatures. The main driving force for this phenomenon is interface energy [12].

3.2. Mechanical properties evaluation

Fig. 8 illustrates the stress-strain curves for as-received, H1 treated, H1+20% cold work+Age1 and H1+HF7+20% cold work+Age2 specimens. The solution heat treatment gives a metastable solid solution matrix that has the highest elongation and lowest tensile strength. As mentioned above, cold working increases the strength and decreases the elongation through the dislocation density and twin's intersection enhancement [27]. In order to achieve an appropriate ductility without dropping the strength down, hot deformation seems to be an intransitive stage of the perfect material fabrication. Hot deformation results in more uniform distributed fine grains, which leads to an increase in the strength without remarkable reduction of ductility [20]. On the other hand, hot deformation, as a thermo-mechanical processing, consumes high density of dislocation and twin boundaries to grow the dynamically recrystallized grains. This leads to higher ductility and lower hardness after hot deformation, which would lead to further cold working to achieve higher hardness and strength. The Age1 and Age2 have been selected as the proper aging conditions because they have increased the microhardness to an industrial specification requirement. The longer time for thermal exposure during hot deformation and aging increases the amount of $M_{12}C$ carbides which improves the elongation by hindering the crack propagation [16]. Fig. 9 also shows the fracture surface of as-received, H1+20% cold work+Age1 and H1+HF7+20% cold work+Age2 specimens.
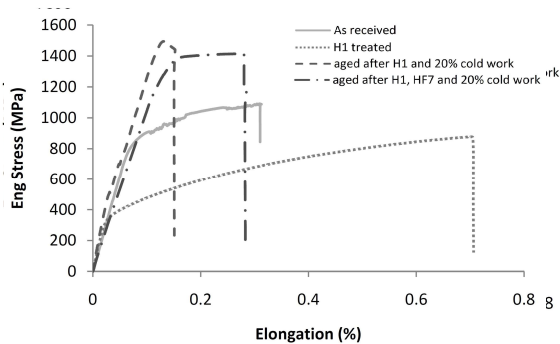

Fig. 8. The stress-strain curves for as-received, H1 treated, H1+20% cold work+Age1 and H1+HF7+20% cold work+Age2 specimens.
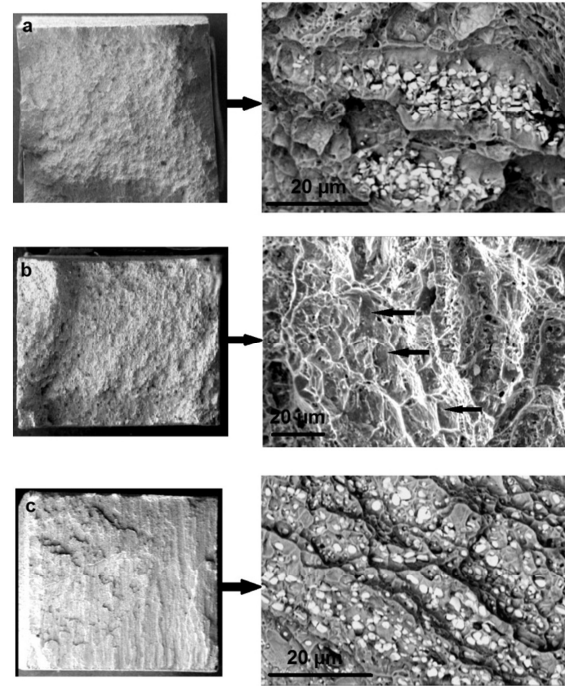

Fig. 9. Tensile fracture surface of a) as-received, b) H1+ 20% cold worked+Age1 and c) H1+HF7+20% cold work+Age2 specimens.

The as-received sample (Fig. 9(a)) shows a mixed ductile-brittle fracture surface. Plastic deformation has taken place in the precipitation free zones and wherever second phase particles are present, the mechanism has changed to the brittle fracture. The segregated fractured M_6C and $M_{23}C_6$ carbides are not coherent with the matrix in comparison with the MC and $M_{12}C$ carbides. Therefore, they might easily be the sources of crack initiation and lead to reducing the ductility [16]. The cold worked sample (Fig. 9(b)) has experienced lower plastic deformation and brittle fracture seems to be the prevailing mechanism. The intergranular planar slip bands, due to cold working and former dislocations, act as the constraints against the dislocation movement. This would increase the hardness and tensile strength. The hot deformed specimen (Fig. 9(c)) shows a higher degree of plastic deformation than that of the cold worked sample (Fig. 9(b)). The right hand back scattered SEM image indicates the uniform distribution of reinforcement particles and plastic deformation. The uniformly distributed second phase particles act as void-nucleation sites on the one hand and prevent the voids

Table 5. Microhardness of samples after different processing route

Sample's condition	Hardness (VHN) ±5	Sample's condition	Hardness (VHN) ±5
As-received	502	H1+HF4	493
H1	321	H1+HF5	460
H2	301	H1+HF6	510
H3	262	H1+HF7	310
H4	279	H1+HF8	344
H1+20% cold work	542	H1+HF9	409
H1+20% cold work+Age1	573	H1+HF7+20% cold work+Age1	433
H1+HF1	441	H1+HF7+20% cold work+Age2	445
H1+HF2	404	H1+HF7+20% cold work+Age3	479
H1+HF3	488	H1+HF7+20% cold work+Age4	451

From coalescence on the other. The cold worked sample's shallow dimples are a little elongated in comparison with the hot forged samples. It is attributed to the activation of tear or shear loading condition in the last steps of fracture. The first steps have started with quasi-cleavage fracture. The large dimples elongated from cleavage facets verify the occurrence of this mechanism. The dipper dimples of hot worked sample, including the serpentine glide lines, confirm the activation of the plastic deformation [28].

Microhardness data of different samples are shown in Table 5. There are usually several strengthening mechanisms, including precipitation hardening, solid solution strengthening, grain boundary hardening, and annealing twin's boundary hardening in superalloys [29]. Solution treatment dissolves the precipitations and forms a supersaturated solid solution which has a lower hardness than particle reinforced state. In fact, solution treatment has eliminated the hardening effect of precipitations and appended solid solution and annealing twin's strengthening effects. The second phase particles might pin the grain boundaries and dislocations and enhance the resistance of material to the bulk and localized plastic deformation. Increasing the time and temperature of age hardening treatment would increase the particle size and increase the hardness to the maximum value, at most. After a certain period of the time, over-aging will take place and the hardness will decrease.

Hot deformation refines the grain structure and increases the hardness based on the Hall-Petch relationship. Hot deformation temperature also influences the dissolution of the precipitations. Higher hot deformation temperatures activate more restoration mechanisms resulting in a lower hardness. The optimum manufacturing process and related parameters should be selected based on the final expected microstructure, mechanical properties, and other desired properties.

Table 6 represents the impact energy of different samples. As discussed before, dynamic recrystallization, due to hot deformation forms finer grain structures, distribute the second phase uniformly and break the as-cast segregated structure which can be an appropriate nucleation site for crack initiation and propagation during impact loading. As seen, the nearest impact energy to the solution treated sample belongs to the hot deformed sample. The solution treatment gives a soft

Table 6. Impact energy after different manufacturing conditions

Sample's condition	Charpy impact energy (J) ±4
As-received	44.8
H1	200
H1+20% cold work+Age1	167.7
H1+HF7+20% cold work+Age1	184

energy. The cold worked sample, which has not and precipitation-free matrix with the highest impact experienced hot deformation, has the lowest impact energy after the as-received sample, largely due to higher grain size, non–uniformly distributed particles, and higher dislocation density.

4. Conclusion

A heat resistant age-hardenable Co-based superalloy (HAYNES 25) is subjected to the heat treatment, hot deformation, cold working and precipitation hardening processes. The examinations give the following results:

1. In order to break down the inhomogeneous, segregated and bimodal as-cast structure of the HAYNES 25 alloy, the solution treatment seems to be a necessary step, even if the process includes hot deformation. The H1 condition (solution treated at 1230ºC - preheated for 15 min - cooled at 25ºC water) is estimated as the optimum solution treatment process.

2. Based on an industrial application requirement (specified grain size and hardness), the condition HF7 (forged at 1275ºC- strain: 15% - preheated for 20 min - preheated at 1300ºC - cooled at air) is suggested. Hot deformation decreases the grain size, while providing a more homogeneous microstructure and particle's distribution.

3. Given that the hot deformation alone cannot meet the hardness requirements, the cold working process is suggested. 20% cold work increased the hardness to 43-45 HRC (425-445 HVN). In order to use the precipitation's strengthening effect, Age1 and Age2 treatment of Table 4 should be performed. The precipitations keep the strength at higher service temperatures and increase the creep resistant of fabricated components.

4. Based on the specified properties, the H1+HF7+20% cold work+Age1 (aged at 430ºC - hold for 3.5 h - cooled at air) process has been selected to fabricate the perfect material for manufacturing an industrial component (a kind of metal gasket).

5. References

[1] J. Sato, T. Omori, K. Oikawa, I. Ohnuma, R. Kainuma, K. Ishida, Cobalt-base high-temperature alloys, *Journal of Science*, 312(5770) (2006) 90-91.

[2] R. C. Reed, The superalloys: Fundamentals and applications, Cambridge University Press, 2008, pp. 1-32.

[3] D. Ufukerbulut, I. Lazoglu, Biomaterials for Artificial Organs, Woodhead Publishing, 2011, pp. 10-50.

[4] L.M. Pike, 100 years of wrought alloy development at HAYNES, *International Mineral Metallic Materials Society*, 15 (2014).

[5] A. I. H. Committee, ASM handbook: Heat treating, ASM International, 1991.

[6] M. Knezevic, J.S. Carpenter, M.L. Lovato, R.J. McCabe, Deformation behavior of the cobalt-based superalloy HAYNES 25: Experimental characterization and crystal plasticity modeling, *Acta Materialia*, 63 (2014) 162-168.

[7] W.S. Lee, H.C. Kao, High temperature deformation behaviour of HAYNES 188 alloy subjected to high strain rate loading, *Materials Science and Engineering: A,* 594 (2014) 292-301.

[8] Y.T. Zhu, X.Y. Zhang, H.T. Ni, F. Xu, J. Tu, C. Lou, Formation of $\{112\bar{1}\}$ twins in polycrystalline cobalt during dynamic plastic deformation, *Materials Science and Engineering A*, 548 (2012) 1-5.

[9] M.L. Benson, P.K. Liaw, T.A. Saleh, H. Choo, D.W. Brown, M.R. Daymond, E.W. Huang, X.L. Wang, A.D. Stoica, R.A. Buchanan, D.L. Klarstrom, Deformation-induced phase development in a cobalt-based superalloy during monotonic and cyclic deformation, *Physica B: Condensed Matter*, 385 (2006) 523-525.

[10] F. Fellah, G. Dirras, J. Gubicza, F. Schoenstein, N. Jouini, S.M. Cherif, C. Gatel, J. Douin, Microstructure and mechanical properties of ultrafine-grained fcc/hcp cobalt processed by a bottom-up approach, *Journal of Alloys and Compounds*, 489(2) (2010) 424-428.

[11] M.L. Benson, P.K. Liaw, H. Choo, D.W. Brown, M.R. Daymond, D.L. Klarstrom, Strain-induced phase transformation in a cobalt-based superalloy during different loading modes, *Materials Science and Engineering: A*, 528 (2011) 6051-6058.

[12] J. Favre, D. Fabrègue, E. Maire, A. Chiba, Grain growth and static recrystallization kinetics in Co–20Cr–15W–10Ni (L-605) cobalt-base superalloy, *Philosophical Magazine,* 94(18) (2014) 1992-2008.

[13] HAYNES® 25 Alloy, in: H.I. Inc. (Ed.) Heat resistance alloys at a glance, HAYNES INTERNATIONAL Inc., Kokomo, Indiana USA, 2008.

[14] J.R. Davis, A.S.M.I.H. Committee, Nickel, Cobalt, and their alloys, ASM International, 2000.

[15] A.S. Kurlov, A.I. Gusev, Tungsten carbides: Structure, properties and application in hardmetals, Springer, 2013.

[16] T. Liu, J.S. Dong, L. Wang, Z.J. Li, X.T. Zhou, L.H. Lou, J. Zhang, Effect of long-term thermal exposure on microstructure and stress rupture properties of GH3535 superalloy, *Journal of Materials Science Technology*, 31(3) (2015) 269-279.

[17] J. Teague, E. Cerreta, M. Stout, Tensile properties and microstructure of HAYNES 25 alloy after aging at elevated temperatures for extended times, *Metallurgical and Materials Transaction A,* 35(9) (2004) 2767-2781.

[18] J. Favre, Recrystallization of L-605 cobalt superalloy during hot-working process, PhD diss., Lyon, INSA, 2012, pp. 239.

[19] S. Mandal, A.K. Bhaduri, V.S. Sarma, Origin and role of Σ3 boundaries during thermo-mechanical processing of a Ti-modified austenitic stainless steel, *Materials Science Forum,* 702 (2012) 714-717.

[20] F.J. Humphreys, M. Hatherly, Chapter 13-Hot deformation and dynamic restoration, in: F.J.H. Hatherly (Ed.) Recrystallization and Related Annealing Phenomena (Second Edition), Elsevier, Oxford, 2004, pp. 415-420.

[21] B. Paul, R. Kapoor, J.K. Chakravartty, A.C. Bidaye, I.G. Sharma, A.K. Suri, Hot working characteristics of cobalt in the temperature range 600–950°C, *Scripta Materialia,* 60(2) (2009) 104-107.

[22] J.L. Sun, P.W. Trimby, F.K. Yan, X.Z. Liao, N.R. Tao, J.T. Wang, Grain size effect on deformation twinning propensity in ultrafine-grained hexagonal close-packed titanium, *Scripta Materialia,* 69(5) (2013) 428-431.

[23] Y.T. Zhu, X.Z. Liao, X.L. Wu, J. Narayan, Grain size effect on deformation twinning and detwinning, *Journal of Materials Science,* 48(13) (2013) 4467–4475.

[24] R.K. Gupta, M.K. Karthikeyan, D.N. Bhalia, B.R. Ghosh, P.P. Sinha, Effect of microstructure on mechanical properties of refractory Co-Cr-W-Ni alloy, *Metals Science and Heat Treatment,* 50(3) (2008) 175-179.

[25] S. Zangeneh, H. Farhangi, Influence of service-induced microstructural changes on the failure of a cobalt-based superalloy first stage nozzle, *Materials and Design,* 31(7) (2010) 3504-3511.

[26] J.H. Shin, J.W. Lee, Effects of twin intersection on the tensile behavior in high nitrogen austenitic stainless steel, *Materials Characterization,* 91 (2014) 19-25.

[27] F.J. Humphreys, M. Hatherly, Chapter 2-The deformed state, in: F.J.H. Hatherly (Ed.) Recrystallization and Related Annealing Phenomena (Second Edition), Elsevier, Oxford, 2004, pp. 11-12.

[28] Committee AIH, ASM Handbook: Fractography, ASM International, 1987.

[29] T. Osada, N. Nagashima, Y. Gu, Y. Yuan, T. Yokokawa, H. Harada, Factors contributing to the strength of a polycrystalline nickel–cobalt base superalloy, *Scripta Materialia,* 64(9) (2011) 892-895.